

Supplementary Information for

A modeling study of the nonlinear response of fine particles to air pollutant emissions in the Beijing-Tianjin-Hebei region

Bin Zhao^{1,2,3}, Wenjing Wu^{1,2}, Shuxiao Wang^{1,2}, Jia Xing^{1,2}, Xing Chang^{1,2}, Kuo-Nan Liou³, Jonathan H. Jiang⁴, Yu Gu³, Carey Jang⁵, Joshua S. Fu⁶, Yun Zhu⁷, Jiandong Wang^{1,2}, Jiming Hao^{1,2}

[1] School of Environment, and State Key Joint Laboratory of Environment Simulation and Pollution Control, Tsinghua University, Beijing 100084, China

[2] State Environmental Protection Key Laboratory of Sources and Control of Air Pollution Complex, Beijing 100084, China

[3] Joint Institute for Regional Earth System Science and Engineering and Department of Atmospheric and Oceanic Sciences, University of California, Los Angeles, CA 90095, USA

[4] Jet propulsion Laboratory, California Institute of Technology, Pasadena, CA 91109, USA

[5] U.S. Environmental Protection Agency, Research Triangle Park, NC 27711, USA

[6] Department of Civil and Environmental Engineering, University of Tennessee, Knoxville, TN 37996, United States

[7] School of Environmental Science and Engineering, South China University of Technology, Guangzhou 510006, China

Correspondence to: Shuxiao Wang (shxwang@tsinghua.edu.cn)

1 Evaluation of CMAQ/2D-VBS simulations

The meteorological prediction lays the foundation for air quality simulation. In this study, the meteorological parameters simulated by WRFv3.7 are compared with the observational data obtained from the National Climatic Data Center (NCDC), where hourly or 3-h observations are available for 28 sites distributed within the inner domain. Due to the limited observational data available, the statistical evaluation was restricted to the temperature at 2 m, wind speed and wind direction at 10 m, and humidity at 2 m. The statistical indices used include the bias,

gross error (GE), root mean square error (RMSE), systematic RMSE (Sys RMSE), unsystematic RMSE (Unsys RMSE), and index of agreement (IOA). A detailed explanation of these indices can be found in Baker (2004).

Table S3 lists the model performance statistics and the benchmarks suggested by Emery et al. (2001). These benchmark values were derived based on performance statistics of the Fifth-Generation NCAR/Penn State Mesoscale Model (MM5) from a number of studies over the U.S. domain (mostly at grid resolution of 12km or 4km), and have been widely accepted in many regional air quality modeling studies. We expect these standards should also be applicable to our simulation domain. For wind speed, wind direction, and temperature, all statistical indices are within the benchmark range. For humidity, the GE for the July simulation slightly exceeds this benchmark (2.2 g/kg vs 2.0 g/kg) which might be due to the high humidity in summer, while all other statistical indices are within the benchmarks, indicating an acceptable performance. In summary, these statistics indicate an overall decent performance of meteorological predictions.

During the simulation period, the Ministry of Environmental Protection of China (MEP) has been publishing hourly PM_{2.5} concentrations for 138 state-controlled observation sites in the inner domain on its official website (<http://datacenter.mep.gov.cn>). We compare simulated monthly mean PM_{2.5} concentrations with these observations, and employ a number of statistical indices including mean observation, mean simulation, normalized mean bias (NMB), normalized mean error (NME), mean fractional bias (MFB), and mean fractional error (MFE) to give a quantitative assessment of the model performance, as shown in Table S4. The definitions of these indices have been documented in previous papers (Wang et al., 2010; Boylan and Russell, 2006). It can be seen that the PM_{2.5} concentrations are slightly underestimated in all months, with NMBs ranging between -24.8% and -2.6%, probably attributable to the exclusion of fugitive dust emissions. Boylan and Russell (2006) proposed that a model performance goal (the level of accuracy that is considered to be close to the best a model can be expected to achieve) was met if $MFB \leq \pm 30\%$ and $MFE \leq 50\%$, and the model performance criteria (the level of accuracy that is considered to be acceptable for modeling applications) was met if $MFB \leq \pm 60\%$ and $MFE \leq 75\%$. Table S4 shows that all the statistical indices meet the model performance goal, indicating a good modeling performance.

Having compared the monthly average PM_{2.5} concentrations, we continue to evaluate simulated temporal variation of PM_{2.5} concentrations. As described in Section 2.2 in the main text, we define 5 target regions for the development of the ERSM prediction system, i.e.,

1 Beijing, Tianjin, Northern Hebei, Eastern Hebei, and Southern Hebei. We select one
2 representative site in each target region, and compared the hourly PM_{2.5} simulations with
3 observations, as shown in Figs. S1-S5. The figures show that the modeling system can capture
4 the temporal variation of PM_{2.5} concentrations fairly well. The correlation coefficients range
5 between 0.49 and 0.83 in January, March, and October, indicating good model performance.
6 The correlation coefficients are relatively lower in July (0.21-0.49), in association with the
7 relatively large discrepancies in meteorological simulations. Despite the lower correlation
8 coefficients in July, the absolute errors are still acceptable considering the smaller PM_{2.5}
9 concentrations during summer.

10 Furthermore, we compare the simulated concentrations of major PM_{2.5} chemical
11 components with observational data at 7 sites in the inner domain (unpublished data of
12 Tsinghua University). The model performance statistics are summarized in Table S5. NO₃⁻
13 concentrations are overestimated (NMB = 16.3%), while SO₄²⁻ concentrations are
14 underestimated (NMB = -47.5%). There is a 25.1% underestimation in NH₄⁺ concentrations.
15 The overestimation of NO₃⁻ and underestimation for SO₄²⁻ are consistent with previous studies
16 over East Asia, probably attributed to the lack of some chemical formation pathways in the
17 modeling system, such as SO₂ heterogeneous reactions on the dust surface and the oxidation
18 of SO₂ by NO₂ in aerosol water (Fu et al., 2016; Cheng et al., 2016; Wang et al., 2016).
19 Elemental carbon (EC) concentrations are remarkably overestimated by 86.6%. EC
20 concentrations are strongly affected by local emissions, while the spatial distribution of our
21 emission inventory may not sufficiently capture local emission sources surrounding
22 observational sites, leading to model-observation discrepancy. The overestimation may also
23 be attributable to the absence of EC aging in CMAQ/2D-VBS, which leads to reduced
24 fraction of hydrophilic EC and thus reduced wet deposition. Finally, concentrations of organic
25 carbon (OC) are underestimated by 36.8%, although the CMAQ/2D-VBS model has been
26 demonstrated to significantly reduce the underestimation in OC as compared to the default
27 CMAQ model (Zhao et al., 2016). Future studies are needed to further improve the OC
28 simulation results. Similar to the evaluation of PM_{2.5} simulations, we also adopt the
29 benchmarks proposed by Boylan and Russell (2006). Since Boylan and Russell (2006)
30 suggested that less abundant species would have less stringent performance goals and criteria
31 than PM₁₀/PM_{2.5}, we just adopt the model performance criteria (MFB ≤ ±60% and MFE ≤
32 75%) described above. Table S5 shows that all the statistical indices meet the model
33 performance criteria, indicating an overall decent model performance.

2 Selection of heavy-pollution episodes

We collect hourly $\text{PM}_{2.5}$ concentrations at 138 state-controlled monitoring sites over the Beijing-Tianjin-Hebei (BTH) region during 2013-2015 from the Ministry of Environmental Protection (MEP) data center (<http://datacenter.mep.gov.cn/>). The daily-average $\text{PM}_{2.5}$ concentrations for each prefecture-level city are subsequently calculated. For any given day, it is regarded as a regional heavy-pollution day if over 75% prefecture-level cities have daily-average $\text{PM}_{2.5}$ concentrations larger than $75 \mu\text{g}/\text{m}^3$. If three or more continuous days are identified as heavy-pollution days, these days are treated as a regional heavy-pollution episode. In total, 47 regional heavy-pollution episodes are selected.

We subsequently employ the HYSPLIT model (Hybrid Single Particle Lagrangian Integrated Trajectory Model) to identify potential source regions of the heavy-pollution episodes. The HYSPLIT model provides the best-guess transport trajectory for an air parcel to arrive at a target location, based on meteorological data. It has been widely used in atmospheric studies including those conducted in the BTH region (Zhang et al., 2013; Jin et al., 2016; Yao et al., 2016). Since Beijing is located in the central part of the BTH region, we select Beijing urban center (39.95N, 116.43E) as the target location for the calculation of transport trajectory. It is noted, however, the calculated trajectories generally reflect the large-scale meteorological patterns which affects the air pollutant transport over the entire BTH region rather than just Beijing; this can be confirmed from the source attribution results during three typical episodes (Section 3.4 of the main text). For each heavy-pollution day and each of two heights (500 m and 1000 m), the trajectories are simulated at four time points, i.e., 0:00, 6:00, 12:00, and 18:00. Each trajectory is calculated for the last 72 hours at 1-h time resolution. The model is driven by meteorological fields obtained from NCEP GDAS (Global Data Assimilation System) at $1^\circ \times 1^\circ$ resolution. While the HYSPLIT model can only calculate the transport trajectories, the Concentration Weighted Trajectory (CWT) method, an improved back trajectory method, enables a quantitative estimation of the contribution from various source regions (Wang et al., 2015). On the basis of the HYSPLIT simulation results, we further use the CWT method to estimate the contribution of each source region to $\text{PM}_{2.5}$ concentrations at the target location.

Table S7 summarizes the potential source regions of the 47 heavy-pollution episodes. It is clear that the source regions with the highest occurrence frequencies are South (74.5%), Local (57.4%), Northwest (29.8%), Southeast (10.6%), West (8.5%), and North (4.3%). In this study, we selected (1) January 5-7, 2014, (2) October 7-11, 2014, and (3) October 29-31,

2014 as representatives for the Local, South, and Southeast types. For the heavy-pollution episodes with major contribution from the Northwest, our back trajectory analysis indicate that the air mass usually originates from some desert regions. We do not include this type in our analysis because (1) such dust episodes dominated by coarse particles are different from the haze episodes this paper focuses on; (2) the ERSM prediction system developed in this study mainly covers the BTH region, and the long-range transport from the northwestern provinces is beyond the focus of this study.

References

- Baker, K.: Meteorological Modeling Protocol for Application to PM_{2.5}/Haze/Ozone Modeling Projects[R/OL]: http://www.epa.state.oh.us/portals/27/SIP/Attain/D8_Meteorological_Modeling_Protocol.pdf, access: 2015-03-01, 2004.
- Boylan, J. W., and Russell, A. G.: PM and light extinction model performance metrics, goals, and criteria for three-dimensional air quality models, *Atmos Environ*, 40, 4946-4959, DOI 10.1016/j.atmosenv.2005.09.087, 2006.
- Cheng, Y. F., Zheng, G. J., Wei, C., Mu, Q., Zheng, B., Wang, Z. B., Gao, M., Zhang, Q., He, K. B., Carmichael, G., Pöschl, U., and Su, H.: Reactive nitrogen chemistry in aerosol water as a source of sulfate during haze events in China, *Sci Adv*, 2, e1601530, DOI: 10.1126/sciadv.1601530, 2016.
- Emery, C., Tai, E., and Yarwood, G.: Enhanced meteorological modeling and performance evaluation for two Texas episodes. Report to the Texas Natural Resources Conservation Commission: <http://www.tceq.state.tx.us/assets/public/implementation/air/am/contracts/reports/mm/EnhancedMetModelingAndPerformanceEvaluation.pdf>, access: 2015-03-01, 2001.
- Fu, X., Wang, S. X., Chang, X., Cai, S. Y., Xing, J., and Hao, J. M.: Modeling analysis of secondary inorganic aerosols over China: pollution characteristics, and meteorological and dust impacts, *Sci Rep-Uk*, 6, 10.1038/srep35992, 2016.
- Jin, X. C., Xiao, C. J., Li, J., Huang, D. H., Yuan, G. J., Yao, Y. G., Wang, X. H., Hua, L., Zhang, G. Y., Cao, L., Wang, P. S., and Ni, B. F.: Source apportionment of PM_{2.5} in Beijing using positive matrix factorization, *Journal of Radioanalytical and Nuclear Chemistry*, 307, 2147-2154, 10.1007/s10967-015-4544-0, 2016.
- Wang, G. H., Zhang, R. Y., Gomez, M. E., Yang, L. X., Zamora, M. L., Hu, M., Lin, Y., Peng, J. F., Guo, S., Meng, J. J., Li, J. J., Cheng, C. L., Hu, T. F., Ren, Y. Q., Wang, Y. S., Gao, J., Cao, J. J., An, Z. S., Zhou, W. J., Li, G. H., Wang, J. Y., Tian, P. F., Marrero-Ortiz, W., Secrest, J., Du, Z. F., Zheng, J., Shang, D. J., Zeng, L. M., Shao, M., Wang, W. G., Huang, Y., Wang, Y., Zhu, Y. J., Li, Y. X., Hu, J. X., Pan, B., Cai, L., Cheng, Y. T., Ji, Y. M., Zhang, F., Rosenfeld, D., Liss, P. S., Duce, R. A., Kolb, C. E., and Molina, M. J.: Persistent sulfate formation from London Fog to Chinese haze, *P Natl Acad Sci USA*, 113, 13630-13635, 10.1073/pnas.1616540113, 2016.
- Wang, L. T., Jang, C., Zhang, Y., Wang, K., Zhang, Q. A., Streets, D., Fu, J., Lei, Y., Schreifels, J., He, K. B., Hao, J. M., Lam, Y. F., Lin, J., Meskhidze, N., Voorhees, S., Evarts, D., and Phillips, S.: Assessment of air quality benefits from national air pollution

1 control policies in China. Part II: Evaluation of air quality predictions and air quality
2 benefits assessment, *Atmos Environ*, 44, 3449-3457, DOI 10.1016/j.atmosenv.2010.05.058,
3 2010.

4 Wang, Y., Wang, G. C., and Chen, L.: Transportation source and transportation process of
5 PM10 and PM2.5 in seasons of Jinan, *Environ Sci Technol*, 38, 175-182, 2015.

6 Yao, L., Yang, L. X., Yuan, Q., Yan, C., Dong, C., Meng, C. P., Sui, X., Yang, F., Lu, Y. L.,
7 and Wang, W. X.: Sources apportionment of PM2.5 in a background site in the North
8 China Plain, *Sci Total Environ*, 541, 590-598, 10.1016/j.scitotenv.2015.09.123, 2016.

9 Zhang, R., Jing, J., Tao, J., Hsu, S. C., Wang, G., Cao, J., Lee, C. S. L., Zhu, L., Chen, Z.,
10 Zhao, Y., and Shen, Z.: Chemical characterization and source apportionment of PM2.5 in
11 Beijing: seasonal perspective, *Atmos Chem Phys*, 13, 7053-7074, 10.5194/acp-13-7053-
12 2013, 2013.

13 Zhao, B., Wang, S. X., Donahue, N. M., Jathar, S. H., Huang, X. F., Wu, W. J., Hao, J. M.,
14 and Robinson, A. L.: Quantifying the effect of organic aerosol aging and intermediate-
15 volatility emissions on regional-scale aerosol pollution in China, *Sci Rep-Uk*, 6,
16 10.1038/srep28815, 2016.

17
18

1 **Tables and figures**

2 Table S1. Emissions of major air pollutants in prefecture-level cities over the BTH region in
3 2014 (kt yr⁻¹).

	NO _x	SO ₂	NMVOC	NH ₃	PM ₁₀	PM _{2.5}	BC	OC
Beijing	343.6	166.0	357.7	52.2	79.4	55.5	13.3	11.6
Tianjin	344.6	240.3	338.0	45.4	148.2	111.6	16.3	25.8
Shijiazhuang	255.4	169.8	239.7	85.2	198.5	146.1	23.9	33.5
Chengde	76.5	39.6	56.8	32.7	47.4	35.7	6.1	9.7
Zhangjiakou	96.8	46.5	57.2	33.8	52.0	39.5	6.9	11.4
Qinhuangdao	66.7	33.9	52.2	21.8	39.3	29.7	5.3	8.1
Tangshan	247.9	125.8	186.0	66.1	129.3	96.2	15.3	24.1
Langfang	80.5	60.8	104.7	33.8	84.9	62.7	10.5	14.4
Baoding	165.0	107.1	201.5	87.0	151.4	115.4	20.4	32.3
Cangzhou	144.1	102.6	170.0	66.0	144.7	107.0	17.3	24.6
Hengshui	78.4	56.3	93.1	49.1	81.3	60.8	9.8	14.9
Xingtai	142.4	91.6	114.6	58.9	98.7	74.9	12.8	20.9
Handan	198.4	102.2	148.9	80.0	112.3	86.0	14.9	25.5
Total	2240.3	1342.4	2120.4	712.0	1367.5	1021.2	172.7	256.9

4

1 Table S2. Provincial emissions of major air pollutants in China in 2014 (kt yr⁻¹).

	NO _x	SO ₂	NM ₁₀ VOC	NH ₃	PM ₁₀	PM _{2.5}	BC	OC
Beijing	344	166	358	52	79	55	13	12
Tianjin	345	240	338	45	148	112	16	26
Hebei	1552	936	1425	627	1140	854	143	219
Shanxi	934	979	692	197	789	578	127	146
Inner Mongolia	1146	1088	665	366	656	492	112	140
Liaoning	1155	885	1099	382	641	477	68	130
Jilin	656	369	502	272	479	360	52	105
Heilongjiang	755	301	655	346	578	456	78	172
Shanghai	353	528	725	41	141	96	10	9
Jiangsu	1599	983	2085	462	977	707	80	168
Zhejiang	1110	1138	1675	173	443	299	32	50
Anhui	1176	591	1081	417	863	651	91	221
Fujian	799	503	711	167	341	240	28	51
Jiangxi	623	397	499	239	474	312	38	70
Shandong	2717	2334	2529	790	1530	1120	164	258
Henan	1932	1036	1480	954	1379	1004	130	232
Hubei	1234	1201	982	435	877	628	110	171
Hunan	952	839	828	483	792	562	91	151
Guangdong	1685	1032	1683	365	686	478	56	115
Guangxi	736	743	728	352	660	494	46	123
Hainan	139	96	146	59	64	46	4	11
Chongqing	551	998	418	175	352	253	38	71
Sichuan	1172	1661	1282	786	876	671	98	254
Guizhou	676	1062	380	249	565	431	87	137
Yunnan	681	483	449	337	457	339	54	94
Tibet	27	6	16	98	12	9	1	3
Shaanxi	749	748	585	211	527	396	79	127
Gansu	405	286	286	165	307	235	36	69
Qinghai	125	52	61	86	82	62	8	12
Ningxia	210	215	100	40	135	96	14	16
Xinjiang	886	861	405	248	400	296	47	78
Total	27422	22754	24867	9621	17450	12812	1953	3441

2

1 Table S3. Performance statistics for meteorological variables.

Variable	Index	Unit	Jan	Mar	Jul	Oct	Benchmark
Wind Speed	Mean OBS	m/s	2.68	2.95	2.53	2.40	
	Mean SIM	m/s	2.81	3.06	2.66	2.63	
	Bias	m/s	0.13	0.11	0.13	0.24	$\leq \pm 0.5$
	GE	m/s	1.23	1.25	1.19	1.11	≤ 2
	RMSE	m/s	1.86	1.76	1.6	1.58	≤ 2
	Sys RMSE	m/s	1.4	1.12	1.13	1.11	
	Unsys RMSE	m/s	1.2	1.33	1.11	1.10	
	IOA		0.67	0.73	0.65	0.71	≥ 0.6
Wind Direction	Mean OBS	°	230.79	239.51	205.37	195.17	
	Mean SIM	°	249.28	220	201.04	195.10	
	Bias	°	2.99	0.49	-3.45	2.76	$\leq \pm 10$
Temperature	Mean OBS	K	270.3	280.64	298.54	285.70	
	Mean SIM	K	270.03	280.33	298.54	285.92	
	Bias	K	-0.27	-0.3	0	0.21	$\leq \pm 0.5$
	GE	K	1.41	1.66	1.75	1.34	≤ 2
	RMSE	K	1.86	2.28	2.38	1.81	
	Sys RMSE	K	0.43	0.52	0.51	0.47	
	Unsys RMSE	K	1.79	2.21	2.31	1.73	
	IOA		0.97	0.97	0.94	0.97	≥ 0.8
Humidity	Mean OBS	g/kg	1.54	2.83	14	6.02	
	Mean SIM	g/kg	1.66	2.82	13.01	5.49	
	Bias	g/kg	0.12	-0.01	-0.99	-0.53	$\leq \pm 1$
	GE	g/kg	0.32	0.58	2.2	1.01	≤ 2
	RMSE	g/kg	0.47	0.81	2.8	1.38	
	Sys RMSE	g/kg	0.23	0.44	1.76	0.92	
	Unsys RMSE	g/kg	0.4	0.67	2.12	0.96	
	IOA		0.86	0.85	0.76	0.81	≥ 0.6

2

Table S4. Statistical results for the comparison of PM_{2.5} concentrations simulated by CMAQ/2D-VBS with surface observations.

	Jan	Mar	Jul	Oct	Model performance goal ^a	Model performance criteria ^a
Data pairs ^b	3751	3596	3627	4216	-	-
NMB (%)	-24.8	-21.3	-4.2	-2.6	-	-
NME (%)	27.7	24.8	19.3	25.0	-	-
MFB (%)	-29.4	-24.1	-7.8	-1.9	≤ ± 30	≤ ± 60
MFE (%)	33.4	28.7	22.7	24.8	≤ 50	≤ 75
R	0.64	0.73	0.64	0.58	-	-

^a The model performance goals and model performance criteria are adopted from Boylan and Russell (2006).

^b The data used in the statistical analysis are daily PM_{2.5} concentrations.

Table S5. Statistical results for the comparison of PM_{2.5} chemical component concentrations simulated by CMAQ/2D-VBS with observations at 7 surface sites over the BTH region.

	NO ₃ ⁻	SO ₄ ²⁻	NH ₄ ⁺	OC	EC	Model performance criteria ^a
Data pairs ^b	278	278	278	273	271	-
NMB (%)	16.3	-47.5	-25.1	-36.8	86.6	-
NME (%)	67.7	60.6	56.9	52.8	98.6	-
MFB (%)	-2.6	-51.3	-37.7	-48.4	57.2	≤ ± 60
MFE (%)	65.6	76.4	74.2	71.2	67.3	≤ 75
R	0.681	0.637	0.638	0.412	0.389	-

^a The model performance criteria are adopted from Boylan and Russell (2006).

^b The data used in the statistical analysis are daily concentrations of PM_{2.5} chemical components.

Table S6. Description of out-of-sample scenarios

Case number	Description
1-6	Control variables of precursors in Beijing change but the other variables stay the same as the base case. For case 1-3, the emission ratios (defined as the ratios of the changed emissions to the emissions in the base case) of all control variables of precursors in Beijing are set to 0.1, 0.5, and 1.15, respectively. Case 4-6 are generated randomly by applying LHS method for the control variables of precursors in Beijing.
7-12	The same as case 1-6 but for Tianjin.
13-18	The same as case 1-6 but for Northern Hebei.
19-24	The same as case 1-6 but for Eastern Hebei.
25-30	The same as case 1-6 but for Southern Hebei.
31-40	Control variables of precursors change randomly (with LHS method applied) but those of primary inorganic PM _{2.5} stay the same as the base case.
41-44	Control variables of primary inorganic PM _{2.5} change randomly (with LHS method

applied) but those of precursors stay the same as the base case.
 45-54 These cases are generated randomly by applying LHS method for all control variables.

Table S7. Identification of potential source regions for 47 heavy-pollution episodes during 2013-2015 over the BTH region.

NO.	Year	Period	Potential source region
1	2013	January 18-23	Local + Northwest (long distance)
2		January 26-31	Local + South (short distance) + Southeast (short distance)
3		February 23-28	South (short distance) + Northwest (long distance)
4		March 5-8	South (short distance)
5		March 15-18	Local + South (short distance) + Northwest (long distance)
6		April 2-4	Local + South (medium distance) + Northwest (medium distance)
7		May 6-8	South (short distance) + South (medium distance)
8		July 18-20	South (short distance)
9		September 17-19	Local
10		September 27 to October 1	South (short distance)
11		October 4-7	South (short distance)
12		October 30 to November 2	Local + South (short distance) + South (medium distance)
13		November 21-24	Local + Northwest (short distance) + Northwest (medium distance)
14	2014	December 1-4	Local + Northwest (short distance) + North (short distance)
15		December 6-8	Local + South (short distance) + Southeast (short distance)
16		December 21-25	Local + South (short distance)
17		January 5-7	Local + South (short distance)
18		January 13-19	Local + South (short distance)
19		January 22-24	South (short distance)
20		February 11-16	Local + South (short distance) + South (medium distance) + Southeast (short distance)
21		February 20-26	South (short distance) + Southeast (short distance)
22		March 8-11	Local + South (short distance)
23		March 23-28	South (medium distance)
24		March 31 to April 2	Local + South (short distance) + South (medium distance)
25		April 7-9	South (medium distance)
26		April 12-14	South (short distance) + South (medium distance)
27		April 23-25	South (short distance) + South (medium distance)
28		October 7-11	South (short distance) + South (medium distance) + South (long distance)
29		October 17-20	South (short distance) + South (medium distance) + South (long distance)
30		October 23-25	Local + South (short distance) + South (medium distance) + Northwest (long distance)
31		October 29-31	South (short distance) + Southeast (short distance)

32		November 19-21	Local + South (short distance) + South (medium distance) + Northwest (long distance)
33		December 26-29	Local + South (medium distance) + West (medium distance) + Northwest (long distance)
34	2015	January 3-5	Local + West (long distance)
35		January 8-10	Local + Northwest (long distance)
36		January 14-16	South (medium distance) + South (long distance)
37		January 22-26	Local + West (long distance)
38		February 19-21	North (medium distance)、South (long distance)
39		March 6-8	Local + West (long distance)
40		March 15-17	Local + Northwest (long distance)
41		April 9-11	Local
42		May 26-28	Local + South (medium distance)
43		October 14-17	South (medium distance) + Northwest (long distance)
44		November 10-15	Local + South (medium distance)
45		November 27 to December 1	South (medium distance) + Northwest (long distance)
46		December 7-10	Local
47		December 21-26	Northwest (long distance)

1

2

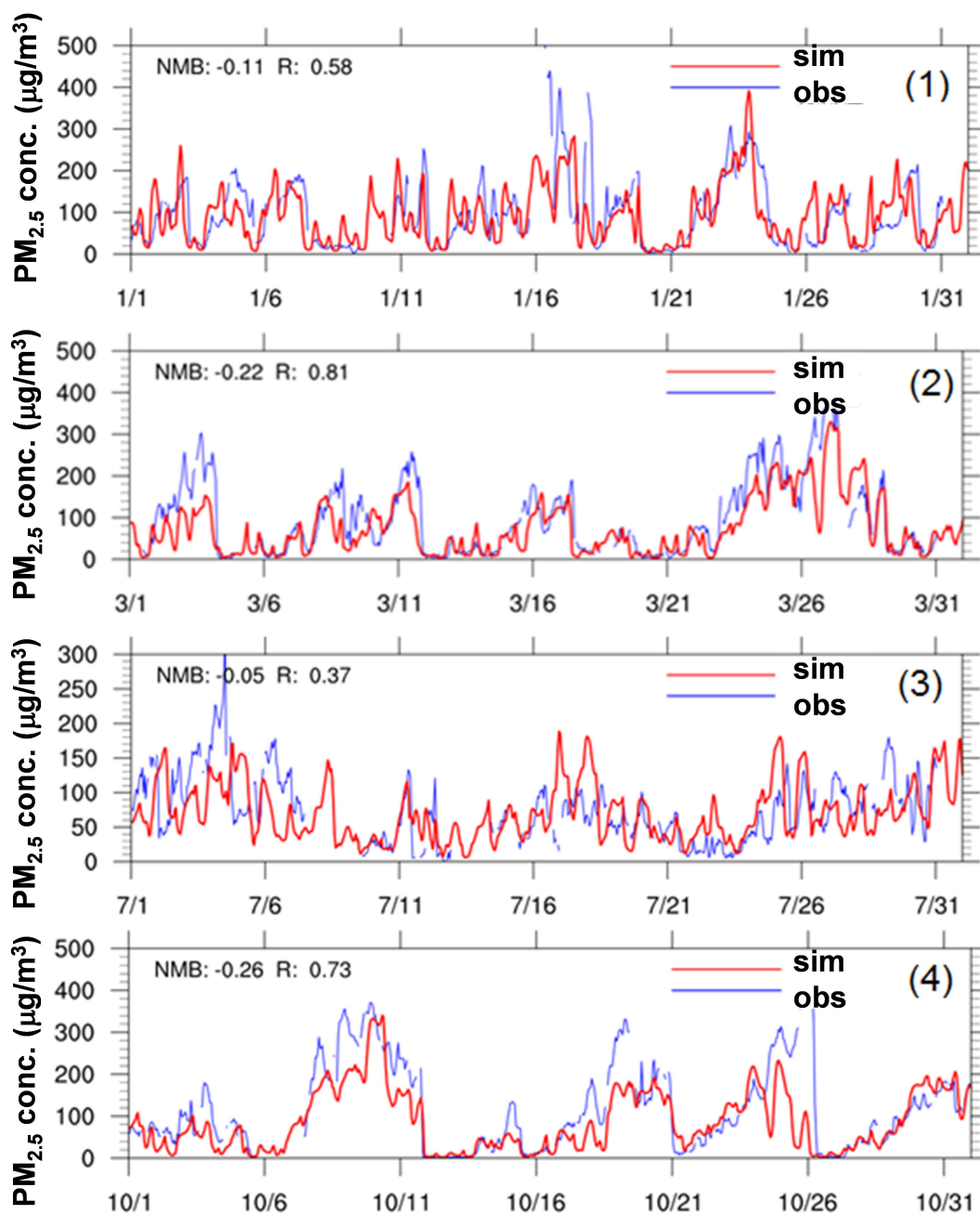


Figure S1. Comparison of simulated and observed $PM_{2.5}$ concentrations at the Dongsi site in Beijing in (1) January, (2) March, (3) July, and (4) October. In July, the simulations and observations are for a nearby Langfang site because the observations at the Dongsi site are missing.

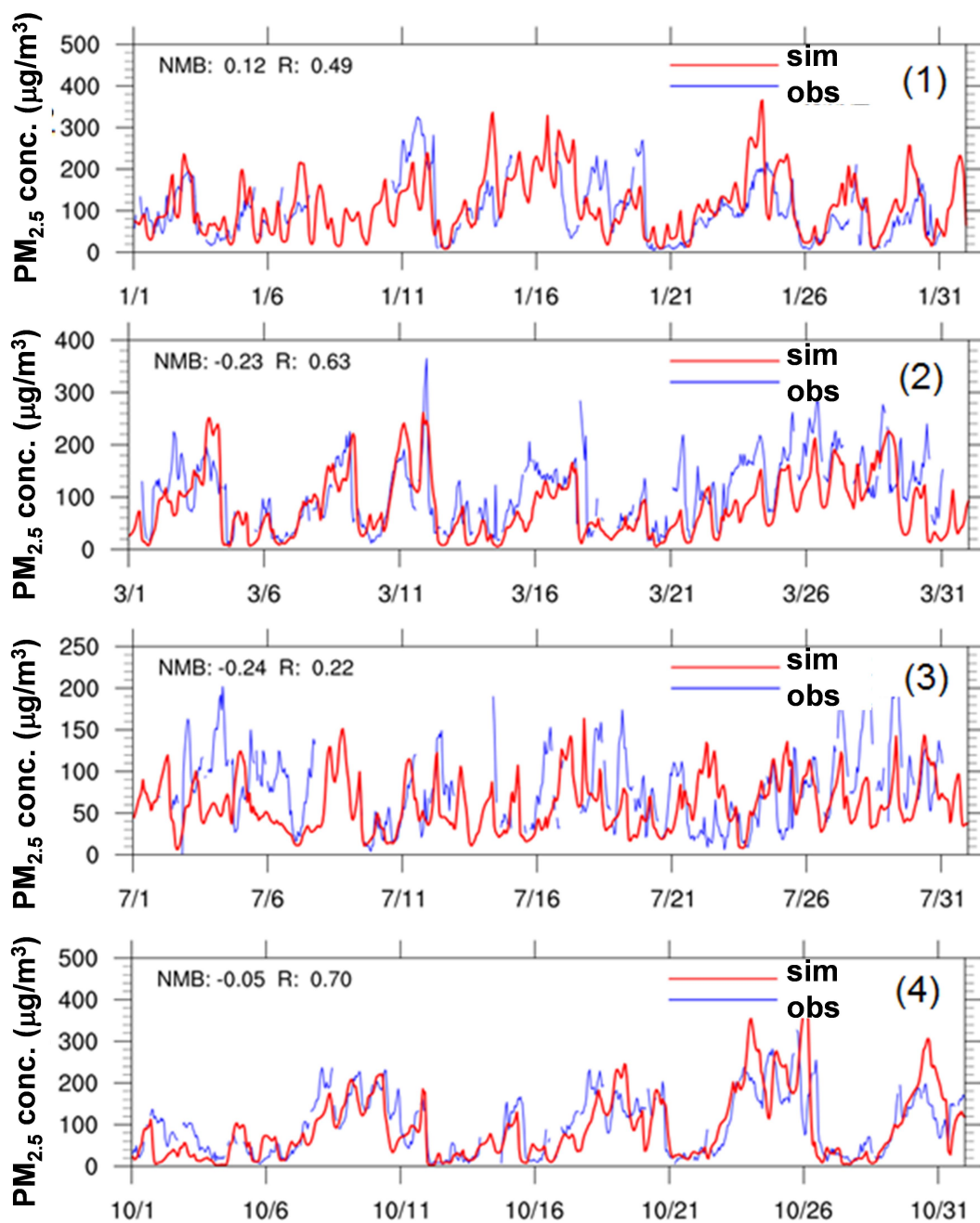


Figure S2. Comparison of simulated and observed PM_{2.5} concentrations at the Tuanbowa site in Tianjin in (1) January, (2) March, (3) July, and (4) October.

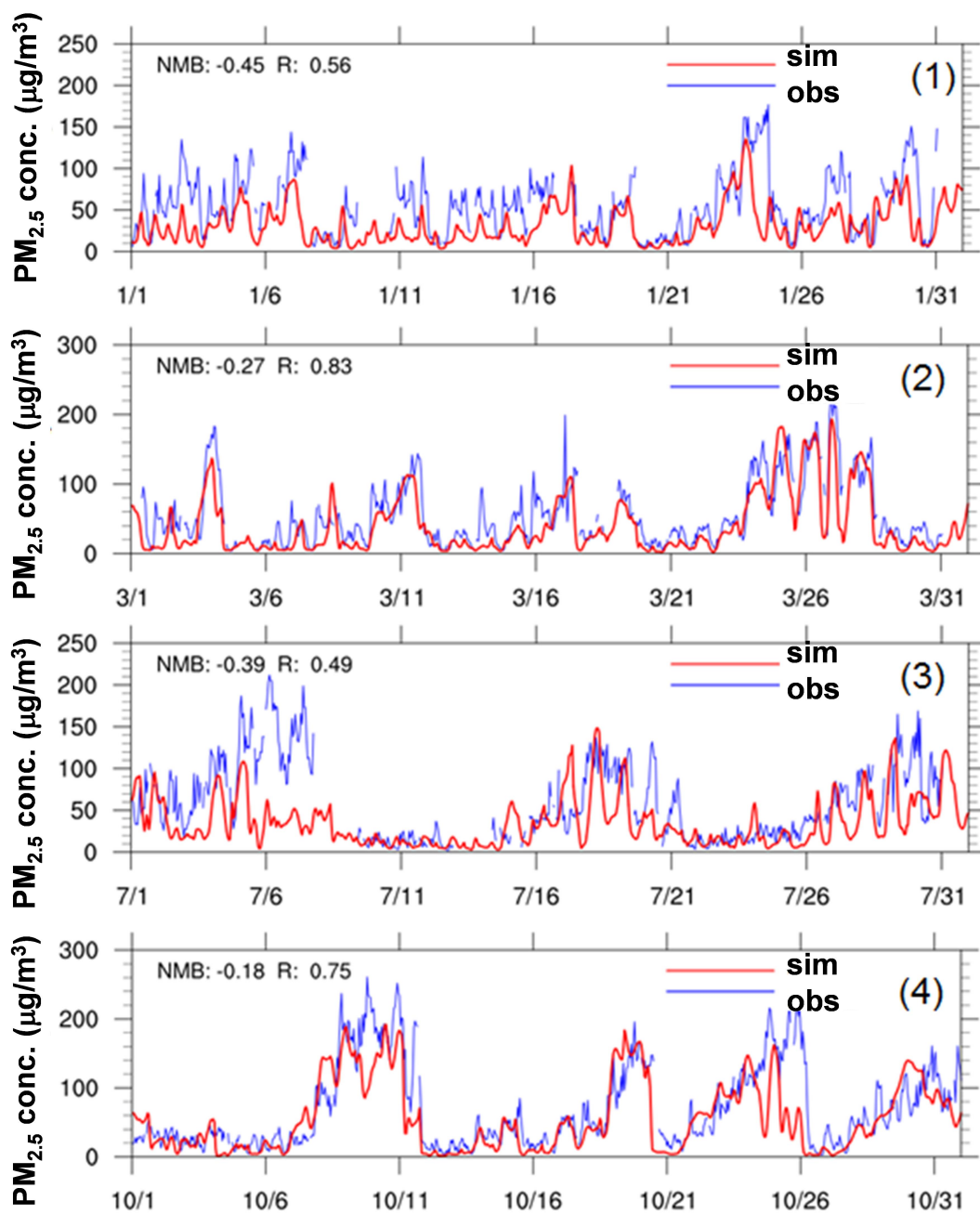


Figure S3. Comparison of simulated and observed PM_{2.5} concentrations at the Chengde site in Northern Hebei in (1) January, (2) March, (3) July, and (4) October.

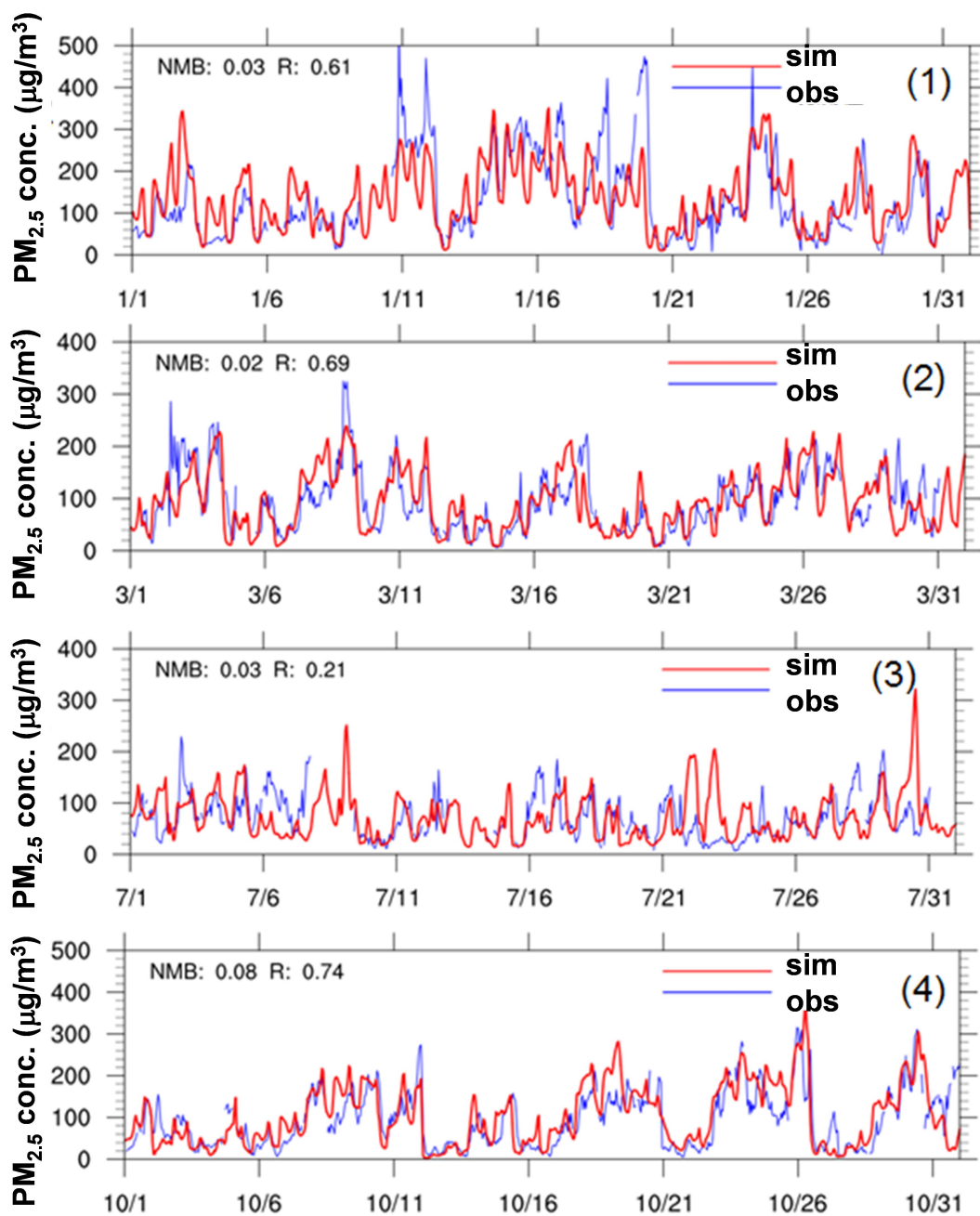


Figure S4. Comparison of simulated and observed PM_{2.5} concentrations at the Cangzhou site in Eastern Hebei in (1) January, (2) March, (3) July, and (4) October.

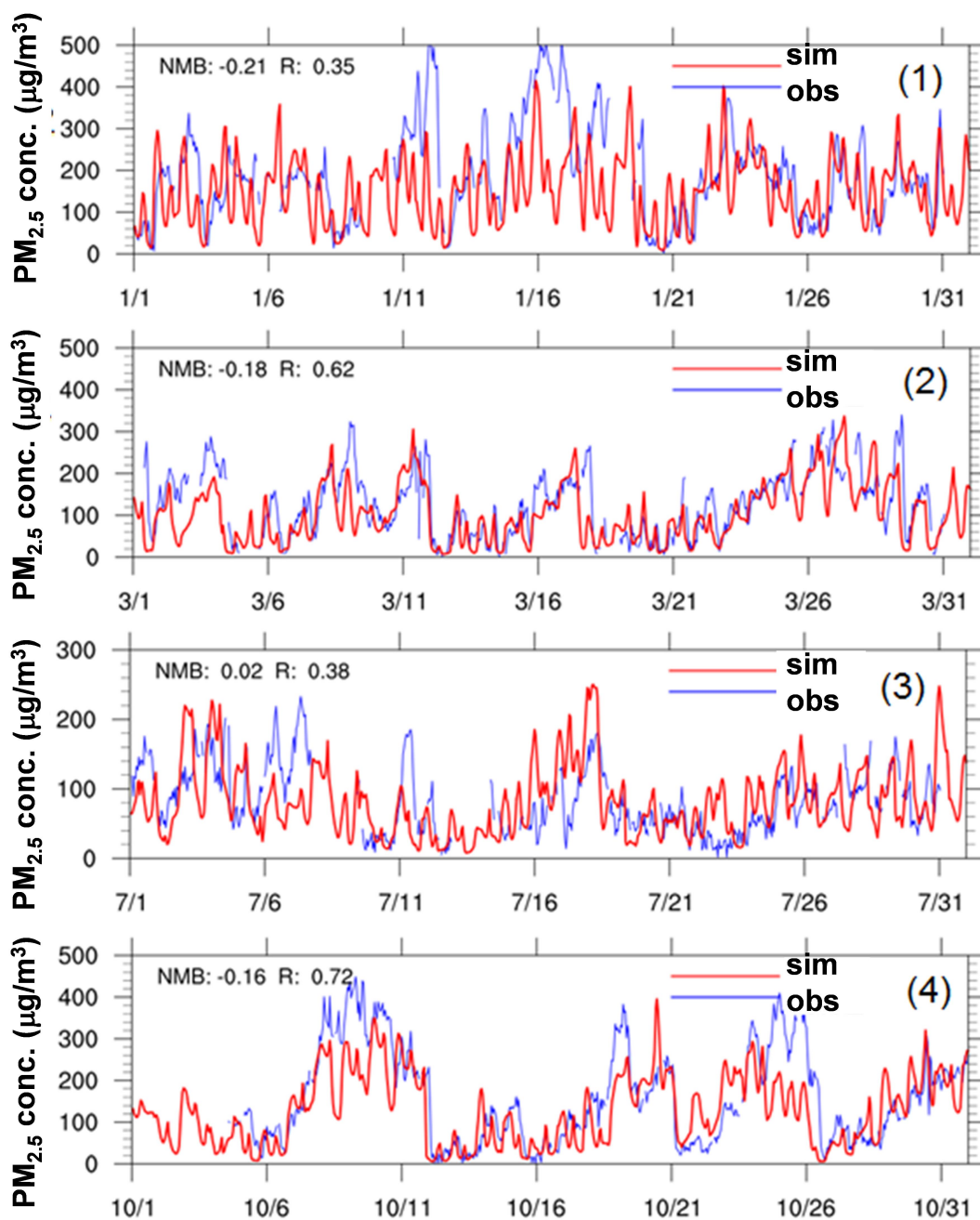


Figure S5. Comparison of simulated and observed $PM_{2.5}$ concentrations at the Baoding site in Southern Hebei in (1) January, (2) March, (3) July, and (4) October.

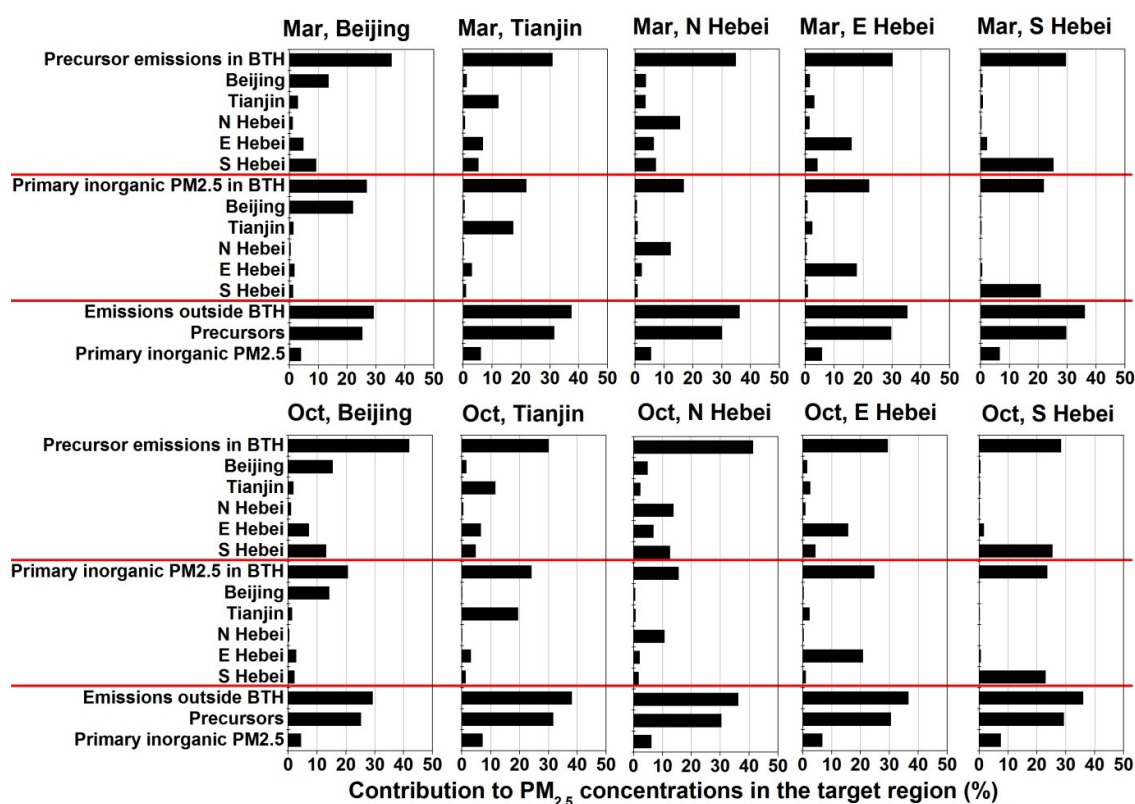
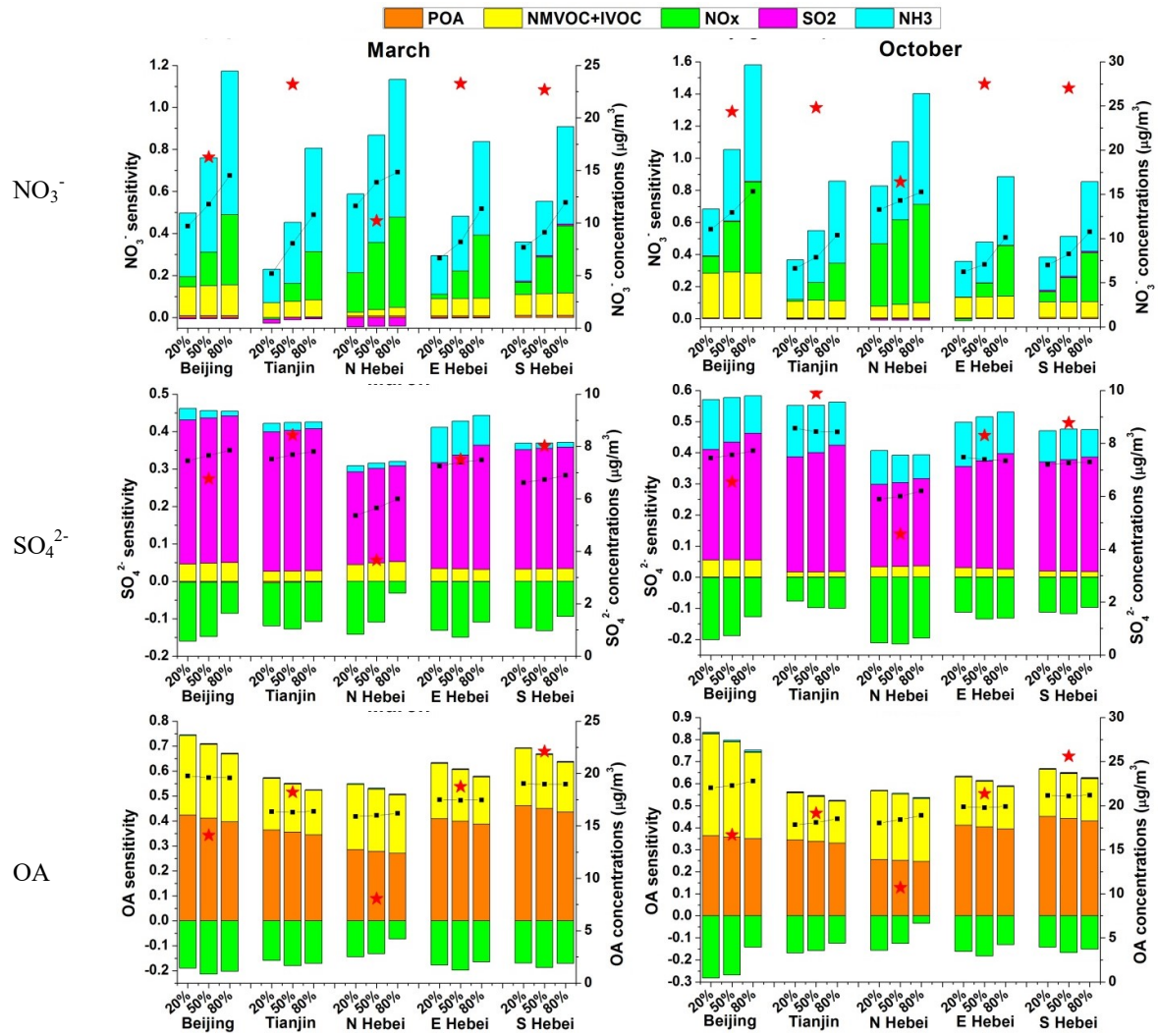


Figure S6. Contributions of precursor (NO_x, SO₂, NH₃, NMVOC, IVOC, and POA) and primary inorganic PM_{2.5} emissions from individual regions to monthly mean PM_{2.5} concentrations in March and October. The contributions are quantified by comparing the base case with sensitivity scenarios in which emissions from a specific source are reduced by 80%. The results for January, July, and the 4-month mean are given in Fig. 6.



1 Figure S7. Sensitivity of monthly mean NO_3^- , SO_4^{2-} , and OA concentrations to stepped
2 control of individual air pollutants in March and October. The meanings of X-axis, Y-axis,
3 coloured bars, black dotted lines, and red stars are the same as Fig. 4 but for $\text{NO}_3^-/\text{SO}_4^{2-}/\text{OA}$.
4 The results for January and July are given in Fig. 7.